Journal of Catalysis 263 (2009) 123–133

Contents lists available at ScienceDirect

Journal of Catalysis

www.elsevier.com/locate/jcat

Characteristics of CeO_2–ZrO_2 mixed oxide prepared by continuous hydrothermal synthesis in supercritical water as support of Rh catalyst for catalytic reduction of NO by CO

Jeong-Rang Kim [a], Wan-Jae Myeong [b], Son-Ki Ihm [a,*]

[a] Department of Chemical and Biomolecular Engineering, Korea Advanced Institute of Science and Technology, 335, Gwahangno, Yuseong-gu, Daejeon 305-701, Republic of Korea
[b] Hanwha Chemical Corporation, 38, Gajeongno, Yuseong-gu, Daejeon 305-804, Republic of Korea

ARTICLE INFO

Article history:
Received 24 September 2008
Revised 19 December 2008
Accepted 2 February 2009
Available online 20 February 2009

Keywords:
CeO_2–ZrO_2
Rh
Co-precipitation
Hydrothermal synthesis
Supercritical water
Oxygen storage/release capacity (OSC)
Thermal stability
Three-way catalysis
NO + CO reaction

ABSTRACT

CeO_2–ZrO_2 mixed oxides were prepared by continuous hydrothermal synthesis in supercritical water (supercritical synthesis) and co-precipitation method, respectively, and they were used as support for Rh catalyst. The activities of Rh-loaded CeO_2–ZrO_2 catalysts were investigated for catalytic reduction of NO by CO and their physicochemical properties were characterized with TPR, N_2 adsorption, O_2-uptake, XRD, Raman, SEM, AES, and H_2/CO chemisorption. Discussions were made on the differences in the catalytic performances between the two preparation methods of CeO_2–ZrO_2 supports in terms of reducibility, homogeneity, morphology, Rh dispersion, and thermal stability. Rh-loaded CeO_2–ZrO_2 prepared by supercritical synthesis showed superior performances for the catalytic reduction of NO by CO as well as better reducibility and higher thermal stability, compared with co-precipitation method, due to its sparsely-agglomerated morphology. CeO_2–ZrO_2 mixed oxide prepared by supercritical synthesis had more potential applications as catalyst support mainly due to its sparsely-agglomerated morphology and higher thermal stability.

1. Introduction

CeO_2–ZrO_2 mixed oxide has potential applications as catalyst support due to its high surface area, thermal stability, and oxygen storage/release capacity (OSC). In addition to the present major use of this material as three-way catalyst promoter, CeO_2- and ZrO_2-based materials have attracted interest in a large variety of catalytic processes [1], ranging from H_2 production from hydrocarbons [2], to sulfur abatement in the fluid catalytic cracking process [3,4], isosynthesis [5], and catalytic water de-pollution [6,7] over recent years.

CeO_2 has the OSC and is widely used as promoter, for example in three-way catalysts to control the automotive gases. CeO_2 acts as an oxygen buffer for three-way catalysts by releasing and uptaking oxygen through redox processes by the Ce^{4+}/Ce^{3+} couple ($CeO_2 \leftrightarrow CeO_{2-x} + (x/2)O_2$), and increase the efficiency of the catalysts by enlarging the air-to-fuel operating window. The role of CeO_2 in three-way catalysis was also suggested to promote the noble metal dispersion; increase the thermal stability of the Al_2O_3 support; promote the water gas shift and steam reforming reactions; favor catalytic activity at the interfacial metal-support sites; promote CO removal through oxidation employing the lattice oxygen [8]. In order to improve the limitation that CeO_2 was sintered at 750 °C [9], some Ce atoms in its crystal lattice were replaced by other cations (such as Zr). This replacement would lead to the microstrain which should improve thermal stability as well as oxygen exchanging ability [10–14].

Continuous hydrothermal synthesis in supercritical water (supercritical synthesis) is a method to prepare metal oxide nanoparticles using supercritical water as antisolvent. When the solution of metal precursors was mixed with supercritical water and heated rapidly, metal oxide nanoparticles could be produced rapidly and continuously by fast hydrolysis and dehydration reaction [15,16]. In our previous work [10], it was confirmed that the supercritical synthesis could lead to CeO_2–ZrO_2 mixed oxide with higher thermal stability and better OSC due to its sparsely-agglomerated morphology, compared with the conventional co-precipitation method.

The catalytic reduction of NO by CO makes a good model reaction for the study of reducing NO_x emissions from automotive gas, and many researches using noble metal catalysts (Rh, Pt and Pd) were reported [17–24]. The noble metals such as Rh also play an important role to improve the reducibility of CeO_2–ZrO_2 mixed oxide because it can activate the reducing agent, i.e. H_2 [25].

* Corresponding author. Fax: +82 42 350 5955.
E-mail address: skihm@kaist.ac.kr (S.-K. Ihm).

0021-9517/$ – see front matter
doi:10.1016/j.jcat.2009.02.001

In this work, CeO_2–ZrO_2 mixed oxides were prepared by supercritical synthesis and co-precipitation method, respectively, and they were used as support for Rh catalyst. The activities of Rh-loaded CeO_2–ZrO_2 catalysts were investigated for catalytic reduction of NO by CO and their physicochemical properties were characterized with TPR, N_2 adsorption, O_2-uptake, XRD, Raman, SEM, AES, and H_2/CO chemisorption. Discussions were made on the differences in the catalytic performances between the two preparation methods of CeO_2–ZrO_2 supports in terms of reducibility, homogeneity, morphology, Rh dispersion, and thermal stability.

2. Experimental

2.1. Sample preparation

$Ce_{0.65}Zr_{0.35}O_2$, which had the highest total OSC among CeO_2–ZrO_2 mixed oxides [10], were prepared by supercritical synthesis and co-precipitation method. In both preparation methods, $ZrO(NO_3)_2$ and $Ce(NO_3)_3$ were used as the precursor of Zr and Ce, while ammonia water as pH controller or precipitator. The detailed processes for both preparation methods as well as the schematic diagram of the apparatus for supercritical synthesis were described elsewhere [10]. The final mixed oxides were obtained only with drying in case of supercritical synthesis, while with further calcination in air flow at 700 °C for 5 h in case of co-precipitation method. The fresh samples prepared by the supercritical synthesis were denoted as "(S)", and those by the co-precipitation method as "(P)".

Rh-loaded CeO_2–ZrO_2 mixed oxides with Rh content of 0.05, 0.1, 0.2, 0.5, and 1 wt% were prepared by incipient wetness impregnation method. The aqueous solution of $Rh(NO_3)_3$ was added to CeO_2–ZrO_2 mixed oxide, followed by drying at 100 °C for 12 h. The samples were calcined in air flow at 600 °C for 3 h.

2.2. Sample characterization

Temperature-programmed reduction (TPR) for Rh-loaded CeO_2–ZrO_2 mixed oxide was carried out in a conventional flow apparatus (Pulsechemisorb 2705, Micromeritics Inc.). A 0.05 g of sample was pretreated in synthetic air flow at 550 °C for 1 h, and cooled in He flow from 150 °C to room temperature for O_2 purge. The sample was then reduced in H_2(5%)/Ar flow with the temperature increasing from room temperature to 1000 °C at a constant heating rate of 10 °C/min. The 4A molecular sieve trap was used to remove the produced H_2O during reduction, and the amount of consumed H_2 was detected using thermal conductivity detector (TCD).

Total OSC of Rh-loaded CeO_2–ZrO_2 mixed oxide, the total amount of O_2 which may be extracted from the sample at a pre-established temperature and partial pressure of the reducing agent (H_2 and CO), was determined by the O_2-uptake. The O_2-uptake of Rh-loaded CeO_2–ZrO_2 mixed oxide was measured in the same apparatus as that of TPR. The sample was reduced in H_2(5%)/Ar flow at 1000 °C for 30 min, and cooled to 427 °C. An oxygen pulse was injected every 3 min to the sample in the main stream of He at 427 °C to obtain the breakthrough curve, from which the total OSC was determined.

The thermal stability of Rh-loaded CeO_2–ZrO_2 mixed oxide could be evaluated by comparing the properties of the sample redox-aged at high temperature with those of the fresh sample. In a conventional flow apparatus, Rh-loaded CeO_2–ZrO_2 mixed oxide was reduced in H_2(5%)/He flow at 1000 °C for 6 h, purged with He for 1 h, and oxidized in O_2(5%)/He flow at 1000 °C for 6 h. The redox-aged samples prepared by the supercritical synthesis were denoted as "(S)_r", and those by the co-precipitation method as "(P)_r".

BET surface area, pore volume, and pore size distribution of Rh-loaded CeO_2–ZrO_2 mixed oxides were measured by N_2 adsorption using ASAP2010 (Micromeritics Inc.). The samples were degassed at 150 °C for ca. 8 h, and N_2 adsorption was carried out at −196 °C.

The crystal structures of Rh-loaded CeO_2–ZrO_2 mixed oxides were confirmed by powder X-ray diffraction (XRD) pattern using monochromic CuK_α radiation (RIGAKU, D/MAX-2500) operating at 40 kV and 300 mA. The average crystallite size of CeO_2–ZrO_2 mixed oxide was also measured by the X-ray line broadening technique employing the Scherrer formula using the profiles of the (1 1 1) peak.

Vis-Raman spectra were obtained at room temperature using a LabRAM HR UV/vis/NIR (Horiba Jobin Yvon) spectrometer with an Ar ion laser of 514.5 nm excitation wavelength. Backscattering geometry was adopted for the measurement under the conditions of a laser power of 25 mW and a resolution of 2 cm^{-1}.

Scanning electron microscope (SEM) images of Rh-loaded CeO_2–ZrO_2 mixed oxides were obtained by a field emission type—SEM (HITACHI S4800) operating at an acceleration voltage of 1.0–2.0 kV. The sample was prepared by sprinkling the powder onto viscous graphite colloidal solution painted on a microscope stub, followed by drying.

For the compositional depth profiles of Rh, auger electron spectroscope (AES) measurements were carried out with SAM4300 (Perkin–Elmer) operating at an acceleration voltage of 5 kV. The cylindrical mirror analyzer (CMA) was used for the detection of emitted auger electron. The powder sample was pressurized to a pellet. The Ar ion beam used to sputter the pellet was operated at an acceleration voltage of 3 kV.

ASAP2010 (Micromeritics Inc.) and Pulsechemisorb 2705 (Micromeritics Inc.) with TCD was used to determine the Rh dispersions. The amount of H_2 adsorbed on Rh was determined on ASAP2010 by H_2 chemisorption at −80 °C [26,27]. The amount of CO adsorbed on Rh was also determined on Pulsechemisorb 2705 by O_2–CO_2–H_2–CO pulse method proposed by Takeguchi et al. [28]. The details of each procedure are explained in the following:

- H_2 chemisorption at −80 °C: The sample (0.5 g) was pretreated in O_2 flow at 550 °C for 1 h, then evacuated at 550 °C for 1 h. The sample was reduced in H_2 flow at 500 °C for 1 h, then evacuated at 400 °C for 4 h. After the sample was cooled down to −80 °C using the cryogen (liquid nitrogen mixed with isopropyl alcohol), H_2 chemisorption was carried out over a range of H_2 pressure of 2–20 Torr.
- O_2–CO_2–H_2–CO pulse method: The catalyst (0.1 g) was degassed in O_2 flow at 300 °C for 1 h, then cooled down to 30 °C and flushed with He for 10 min. TPR was carried out in H_2(5%)/Ar flow at a heating rate of 10 °C/min and was stopped as soon as the end of the first reduction peak. After the sample was cooled down to 30 °C, it was flushed with He for 10 min and was exposed to O_2 flow for 10 min. CO_2 was fed to the sample for 10 min, and then purged with He for 10 min. H_2(5%)/Ar gas was fed to the sample for 10 min, and then purged with He for 1 h. 0.1 mL of CO was pulsed every 3 min until the intensity of the peak was a constant value.

A chemisorption stoichiometry ratio of CO:Rh and H:Rh was assumed to be 1:1 for both cases.

2.3. Catalytic activity measurement

The catalytic activity was measured using a fixed-bed flow reactor at atmospheric pressure. Prior to each reaction, the samples (0.5 g) were pretreated in O_2(5%)/He flow at 550 °C for 2 h. A feed gas mixture of CO(1%), NO(0.1%), and O_2(0.45%) passed

through the catalyst bed (oxidants/reductants stoichiometric factor, $\{2[O_2]+[NO]\}/[CO]=1$), and He was used to balance the total flow rate to 260 mL/min (GHSV = 40000 h^{-1}). Catalyst bed temperature was raised at a rate of 2 °C/min from room temperature to 600 °C under continuous flow of reactant stream. The effluent gas was analyzed by on-line gas chromatographs (column: Molecular Sieve 5A & Porapak Q) equipped with TCD for the analysis of CO, O_2, N_2 and N_2O. NO_x analyzer was employed to analyze the concentration of NO and NO_2. NO conversion to N_2 and N_2O was defined as follows:

NO conversion to N_2 and $N_2O(\%) = 2(C_{N_2,out}+C_{N_2O,out})/C_{NO,in}\times 100$, where $C_{i,in}$ is the concentration of compound i at the reactor inlet and $C_{i,out}$ at the reactor outlet.

3. Results and discussion

3.1. The reducibilities and physical properties of Rh-loaded CeO_2–ZrO_2

TPR results of Rh-loaded CeO_2–ZrO_2 mixed oxides prepared by the supercritical synthesis before redox-aging were compared with those after redox-aging, as shown in Fig. 1. The fresh samples before redox-aging were denoted as "(S)" and the samples after redox-aging as "(S)_r". The noble metals such as Rh play an important role to improve the reducibility of CeO_2–ZrO_2 mixed oxide because it can activate the reducing agent, i.e. H_2 [25]. In comparison with TPR result of CeO_2–ZrO_2 mixed oxide (Fig. 1a), the peak around 800 °C for bulk reduction of CeO_2–ZrO_2 mixed oxide [29,30] remained the same in the TPR results of Rh-loaded CeO_2–ZrO_2 mixed oxides, while the peak around 500 °C for surface reduction of CeO_2–ZrO_2 mixed oxide [29,30] was shifted to around 150 °C due to Rh impregnation [25]. Even if the reduction peaks around 500 °C were retained until the Rh loading less than 0.2 wt%, they were completely shifted beyond 0.5 wt%. The reduction peaks around 150 °C appeared at a lower temperature with higher Rh loading. Like the case of pure CeO_2–ZrO_2 mixed oxide, the peak intensity for bulk reduction around 800 °C decreased and disappeared after redox-aging and the intensity of the reduction peak around 150 °C increased greatly after redox-aging. Additionally, higher Rh loading led to the shift of the reduction peak around 150 °C to lower temperature after redox-aging. It implies that their reducibilities were enhanced significantly after redox-aging especially with higher Rh loading.

TPR results of Rh-loaded CeO_2–ZrO_2 mixed oxides prepared by the co-precipitation method before redox-aging were compared with those after redox-aging, as shown in Fig. 2. The fresh samples before redox-aging were denoted as "(P)" and the samples after redox-aging as "(P)_r". In comparison with TPR result of CeO_2–ZrO_2 mixed oxide (Fig. 2a), the peak around 800 °C for bulk reduction also remained the same in those of Rh-loaded CeO_2–ZrO_2 mixed oxides, while the peak around 500 °C for surface reduction was shifted to around 150 °C due to Rh impregnation. Unlike the case of the supercritical synthesis, the reduction peaks around 500 °C were completely shifted and disappeared in spite of a low Rh loading of 0.05 wt%. However, the reduction peaks around 150 °C were shifted to lower temperature with higher Rh loading. Also, the peaks for bulk reduction around 800 °C still remained even after redox-aging, in contrast with the case of supercritical synthesis. The reduction peaks around 150 °C became broader and lower after redox-aging. It implies that their reducibilities were inhibited after redox-aging, contrary to supercritical synthesis.

Surface area, pore volume, and total OSC of Rh-loaded CeO_2–ZrO_2 mixed oxides before and after redox-aging were shown in Table 1. Rh-loaded CeO_2–ZrO_2 prepared by supercritical synthesis maintained relatively high surface area even after redox-aging. But in case of co-precipitation method, their surface area decreased greatly after redox-aging. It was confirmed that physical property of Rh-loaded CeO_2–ZrO_2 mixed oxide was coincident with that of pure CeO_2–ZrO_2 mixed oxide. Total OSC of Rh-loaded CeO_2–ZrO_2

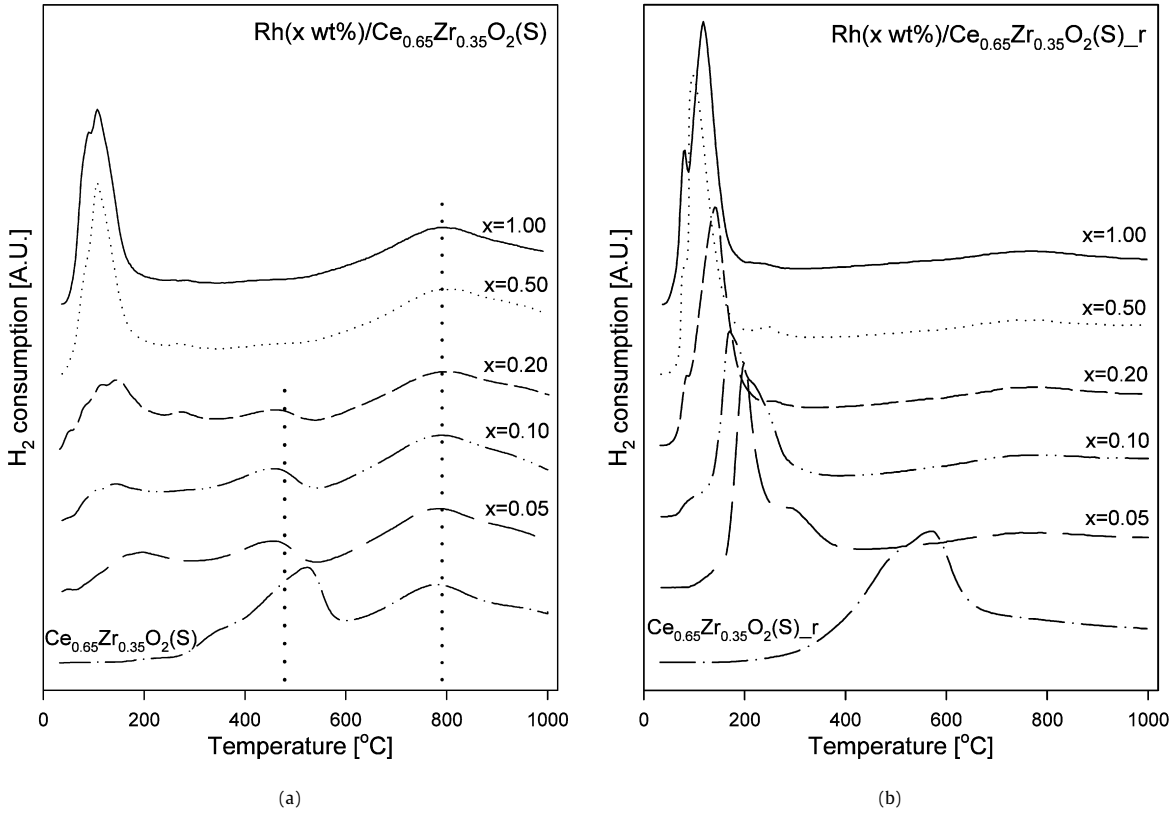

Fig. 1. TPR results of Rh-loaded CeO_2–ZrO_2 mixed oxides prepared by the supercritical synthesis (a) before and (b) after redox-aging.

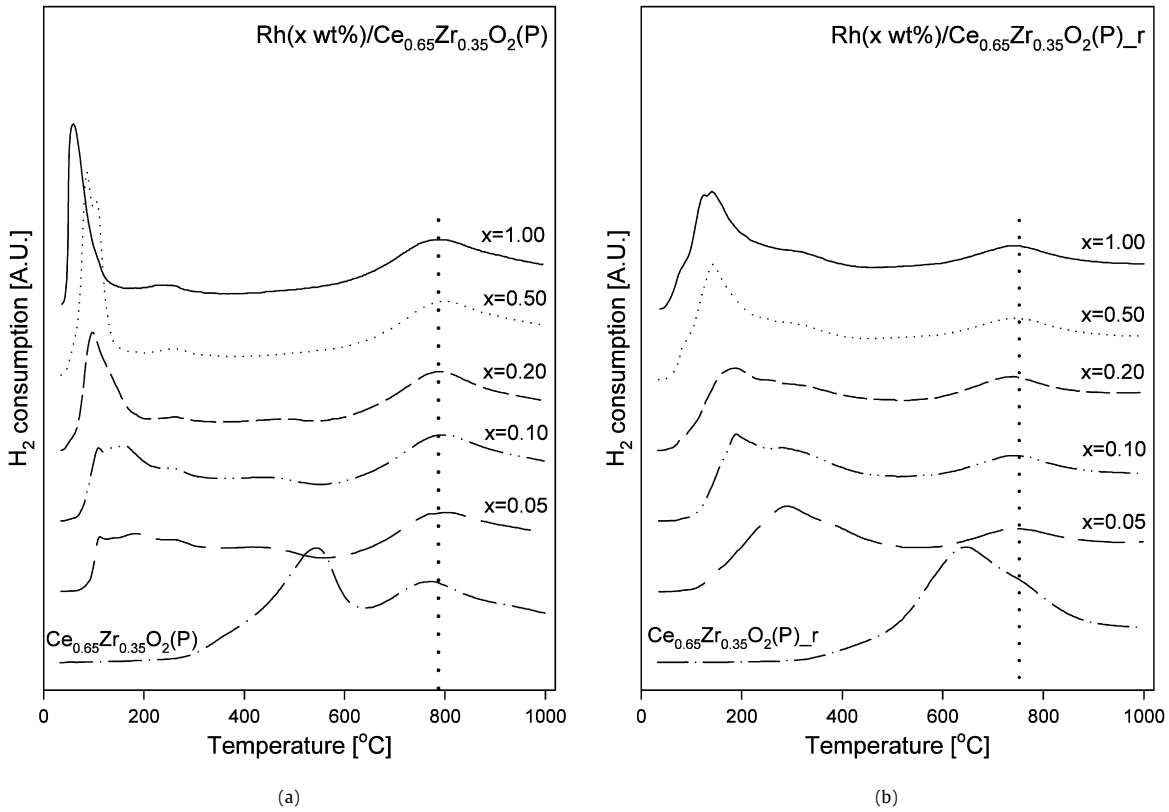

Fig. 2. TPR results of Rh-loaded CeO_2–ZrO_2 mixed oxides prepared by the co-precipitation method (a) before and (b) after redox-aging.

Table 1
BET surface area, pore volume, and total OSC of Rh-loaded CeO_2–ZrO_2 mixed oxides before and after redox-aging.

	BET surface area (m^2/g)		Pore volume (cm^3/g)		Total OSC ($\mu mol_{O_2}/g$)	
	Fresh	Aged	Fresh	Aged	Fresh	Aged
$Ce_{0.65}Zr_{0.35}O_2$(S)	90.4	**20.1**	0.285	0.159	680	600
Rh(0.05 wt%)/$Ce_{0.65}Zr_{0.35}O_2$(S)	92.7	**20.2**	0.266	0.156	737	732
Rh(0.10 wt%)/$Ce_{0.65}Zr_{0.35}O_2$(S)	93.0	**19.8**	0.271	0.171	730	743
Rh(0.20 wt%)/$Ce_{0.65}Zr_{0.35}O_2$(S)	93.1	**20.0**	0.283	0.168	719	749
Rh(0.50 wt%)/$Ce_{0.65}Zr_{0.35}O_2$(S)	86.2	**19.9**	0.262	0.173	722	743
Rh(1.00 wt%)/$Ce_{0.65}Zr_{0.35}O_2$(S)	78.1	**15.9**	0.171	0.118	719	733
$Ce_{0.65}Zr_{0.35}O_2$(P)	55.2	3.8	0.070	0.021	700	330
Rh(0.05 wt%)/$Ce_{0.65}Zr_{0.35}O_2$(P)	56.5	5.3	0.079	0.033	646	710
Rh(0.10 wt%)/$Ce_{0.65}Zr_{0.35}O_2$(P)	56.1	5.1	0.078	0.032	674	677
Rh(0.20 wt%)/$Ce_{0.65}Zr_{0.35}O_2$(P)	55.5	4.7	0.077	0.030	674	707
Rh(0.50 wt%)/$Ce_{0.65}Zr_{0.35}O_2$(P)	55.1	5.3	0.076	0.031	701	694
Rh(1.00 wt%)/$Ce_{0.65}Zr_{0.35}O_2$(P)	53.0	5.6	0.073	0.036	701	686

mixed oxides did not change greatly after redox-aging regardless of the synthesis method.

Like the case of pure CeO_2–ZrO_2 mixed oxide [10], it was confirmed that the supercritical synthesis could lead to Rh-loaded CeO_2–ZrO_2 mixed oxide with better reducibility and higher thermal stability especially through redox-aging treatment.

3.2. The activities for catalytic reduction of NO by CO

Catalytic reduction of NO by CO is an appropriate model reaction for three-way catalysis. The reaction was carried out using typical fixed-bed flow reactor. The activities of Rh-loaded CeO_2–ZrO_2 prepared by supercritical synthesis before and after redox-aging were shown in Fig. 3. From CO conversion to CO_2 and NO conversion to N_2 and N_2O, the activities before and after redox-aging increased with Rh loading from 0.05 to 1.00 wt%. The activities of Rh-loaded CeO_2–ZrO_2 prepared by co-precipitation method before and after redox-aging were shown in Fig. 4. Like the case of supercritical synthesis, the activities before and after redox-aging increased with Rh loading. The temperatures at 90% conversion of CO or NO (T_{90}) for catalytic reduction of NO by CO over Rh-loaded CeO_2–ZrO_2 were compared to confirm the catalytic activity, as shown in Table 2. The decrease in T_{90} with Rh loading was apparent, indicating higher catalytic activity. Naturally, Rh seemed to play an important role as active sites for the catalytic reduction of NO by CO.

The activities of Rh-loaded CeO_2–ZrO_2 with high Rh loading of 1 wt% before redox-aging were compared with those after redox-aging, as shown in Fig. 5. Rh-loaded CeO_2–ZrO_2 prepared by supercritical synthesis had higher activity and the decrease of its activity after redox-aging was smaller than that of co-precipitation method. In other words, higher activity and stability for the catalytic reduction of NO by CO were obtained over Rh-loaded CeO_2–ZrO_2 prepared by supercritical synthesis, as expected from the

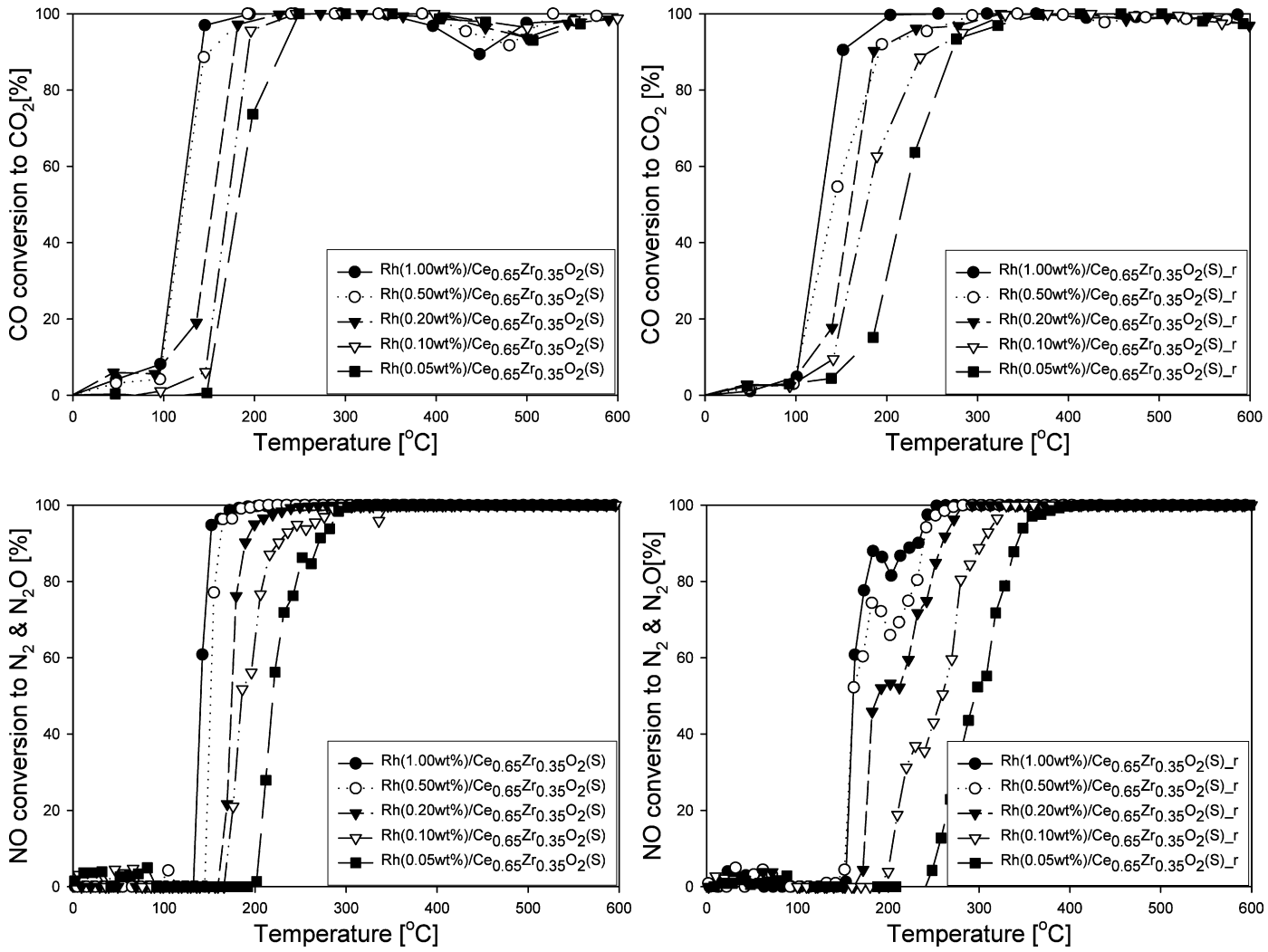

Fig. 3. NO + CO reaction over Rh-loaded CeO_2–ZrO_2 mixed oxides prepared by supercritical synthesis before and after redox-aging.

Table 2
The temperature at 90% conversion of CO or NO (T_{90}) for NO + CO reaction over Rh-loaded CeO_2–ZrO_2 catalysts before and after redox-aging.

	T_{90}, CO		T_{90}, NO	
	Fresh	Aged	Fresh	Aged
Rh(0.05 wt%)/$Ce_{0.65}Zr_{0.35}O_2$(S)	230	272	270	342
Rh(0.10 wt%)/$Ce_{0.65}Zr_{0.35}O_2$(S)	193	248	226	303
Rh(0.20 wt%)/$Ce_{0.65}Zr_{0.35}O_2$(S)	178	187	189	260
Rh(0.50 wt%)/$Ce_{0.65}Zr_{0.35}O_2$(S)	150	192	162	239
Rh(1.00 wt%)/$Ce_{0.65}Zr_{0.35}O_2$(S)	142	152	151	206
Rh(0.05 wt%)/$Ce_{0.65}Zr_{0.35}O_2$(P)	245	292	306	347
Rh(0.10 wt%)/$Ce_{0.65}Zr_{0.35}O_2$(P)	226	278	286	324
Rh(0.20 wt%)/$Ce_{0.65}Zr_{0.35}O_2$(P)	202	260	279	297
Rh(0.50 wt%)/$Ce_{0.65}Zr_{0.35}O_2$(P)	173	224	231	269
Rh(1.00 wt%)/$Ce_{0.65}Zr_{0.35}O_2$(P)	162	214	217	265

discussions in Section 3.1. Accordingly, CeO_2–ZrO_2 mixed oxide, in addition to Rh, seemed to play a role for the catalytic reduction of NO by CO. According to some studies [31–33], it was suggested that the active sites for catalytic reduction of NO by CO are not only Rh metals but also the sites on the support such as Ce sites. CO is chemisorbed over Rh metal and oxidized to CO_2 by oxygen migrated from ceria-related support to Rh metal. NO is reduced to N_2 and N_2O over the reduced Ce site. The oxygen migration provides the way to regenerate the availability of support oxygen vacancies for NO dissociation forming a redox cycle.

3.3. The homogeneity of Rh-loaded CeO_2–ZrO_2

The XRD patterns of CeO_2–ZrO_2 mixed oxides and Rh-loaded CeO_2–ZrO_2 mixed oxides before and after redox-aging were shown in Fig. 6. CeO_2–ZrO_2 mixed oxides prepared by both supercritical synthesis and co-precipitation method had the same crystal structure as cubic phase of CeO_2. In case of both synthesis methods, the characteristic peak of CeO_2–ZrO_2 mixed oxides ((1 1 1) peak → 28.7°) was progressively shifted to larger angles than that of CeO_2 ((1 1 1) peak → 28.6°). This is due to the contraction of lattice cell parameter by insertion of ZrO_2 into CeO_2 fluorite lattice [10,11,34]. The XRD patterns of Rh-loaded CeO_2–ZrO_2 mixed oxides showed the same patterns as CeO_2–ZrO_2 mixed oxides prepared by two synthesis methods. After redox-aging, Rh-loaded CeO_2–ZrO_2 mixed oxides prepared by two synthesis methods kept their crystal structure, while their characteristic peak became narrower and higher due to particle-sintering during redox-aging (Table 3). None of Rh diffraction peaks was observed in the XRD patterns of both fresh and aged samples, and this is mainly owing to the low loading of Rh metal (<1.0 wt%) or the small particle size below the detection limit of this technique.

Average crystallite size of CeO_2–ZrO_2 mixed oxides and Rh-loaded CeO_2–ZrO_2 mixed oxides before and after redox-aging were shown in Table 3. The average crystallite size of CeO_2–ZrO_2 mixed oxide was measured by the X-ray line broadening technique employing the Scherrer formula using the profiles of the (1 1 1) peak.

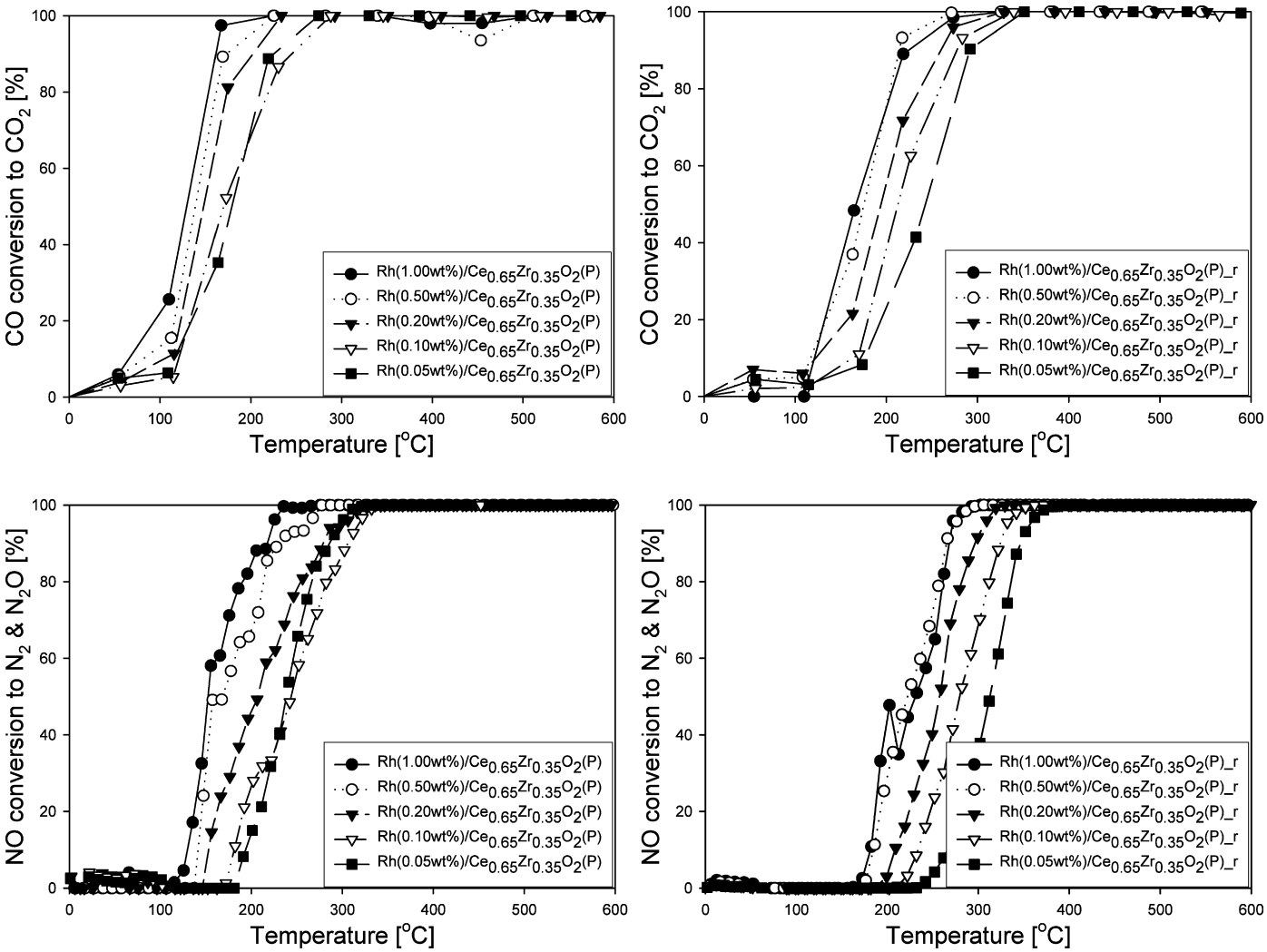

Fig. 4. NO + CO reaction over Rh-loaded CeO_2–ZrO_2 mixed oxides prepared by co-precipitation method before and after redox-aging.

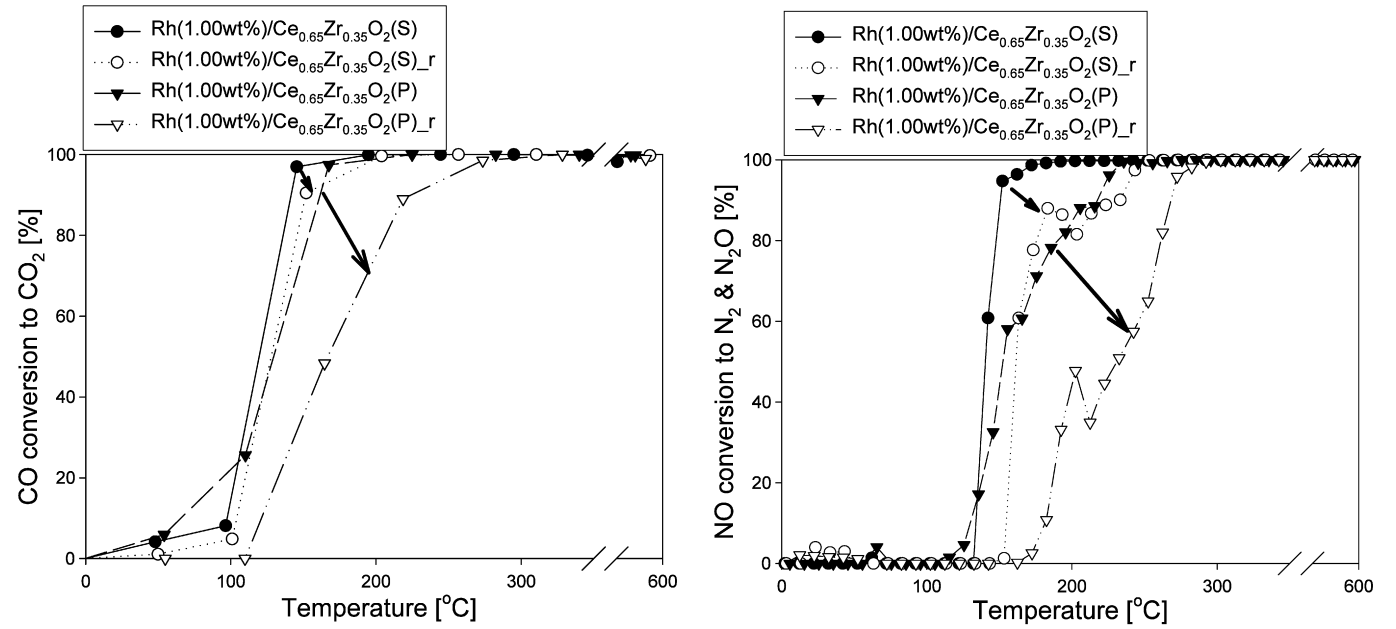

Fig. 5. The comparison of NO + CO reaction over Rh-loaded CeO_2–ZrO_2 mixed oxides with Rh loading of 1 wt% before and after redox-aging.

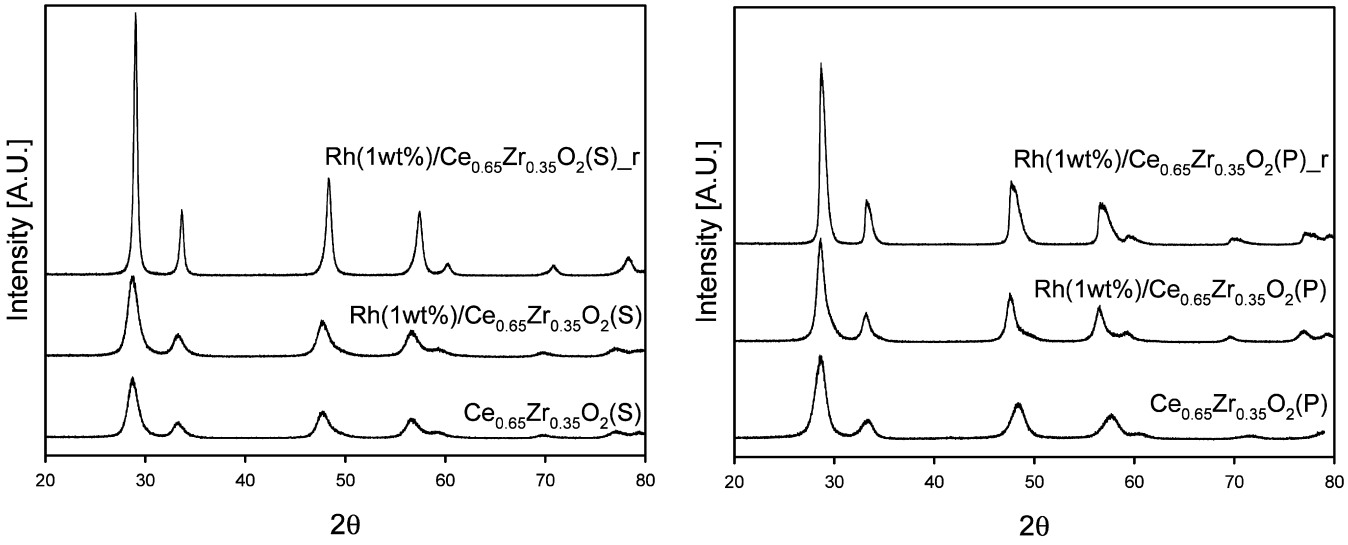

Fig. 6. XRD patterns of CeO_2–ZrO_2 mixed oxides and Rh-loaded CeO_2–ZrO_2 mixed oxides before and after redox-aging.

Table 3
Average crystallite size of CeO_2–ZrO_2 mixed oxides and Rh-loaded CeO_2–ZrO_2 mixed oxides before and after redox-aging.

	Average crystallite size[a] (Å)	
	Fresh	Aged
$Ce_{0.65}Zr_{0.35}O_2$(S)	68	211
Rh(1.00 wt%)/$Ce_{0.65}Zr_{0.35}O_2$(S)	67	193
$Ce_{0.65}Zr_{0.35}O_2$(P)	78	128
Rh(1.00 wt%)/$Ce_{0.65}Zr_{0.35}O_2$(P)	85	138

[a] Calculated by employing the Scherrer formula from the profile of (1 1 1) peak in XRD pattern.

The average crystallite size of CeO_2–ZrO_2 mixed oxides prepared by supercritical synthesis and co-precipitation method was similar with each other and Rh-loaded CeO_2–ZrO_2 mixed oxides had the same average crystallite size as CeO_2–ZrO_2 mixed oxides. It was confirmed that Rh impregnation did not influence the average crystallite size of CeO_2–ZrO_2 mixed oxide. The average crystallite size of Rh-loaded CeO_2–ZrO_2 mixed oxide prepared by supercritical synthesis increased from 67 to 193 Å and that by co-precipitation method from 85 to 138 Å due to crystallite sintering during redox-aging.

Due to nano-sized crystallites of the as-prepared samples, the XRD patterns generally show the broadened peaks which can make it difficult to explore the homogeneity of CeO_2–ZrO_2 mixed oxides. Presence of compositional inhomogeneity facilitates the phase segregation upon calcination and the homogeneity can be better monitored by the XRD patterns of the samples calcined at 900 °C [35–37]. The XRD patterns of CeO_2–ZrO_2 mixed oxides calcined in air flow at 900 °C for 3 h (Fig. 7) showed the presence of a true mixed-oxide phase with the cubic fluorite structure typical of CeO_2 for CeO_2–ZrO_2 mixed oxides prepared by both supercritical synthesis and co-precipitation method. No indication for the presence of other phases was observed. The presence of a cubic-only phase in both samples can indicate that Ce and Zr are homogeneously distributed (if Ce-rich or Zr-rich domains were present, more than one phase would have been formed).

Raman spectroscopy was utilized as an effective tool for confirming the homogeneity of CeO_2–ZrO_2 mixed oxide nanoparticles. The vis-Raman spectra were shown in Fig. 8. CeO_2–ZrO_2 mixed oxides prepared by both supercritical synthesis and co-precipitation method showed one strong Raman peak at 469 cm^{-1} (F_{2g} mode of cubic CeO_2) and a weak band at ca. 620 cm^{-1}, attributed to

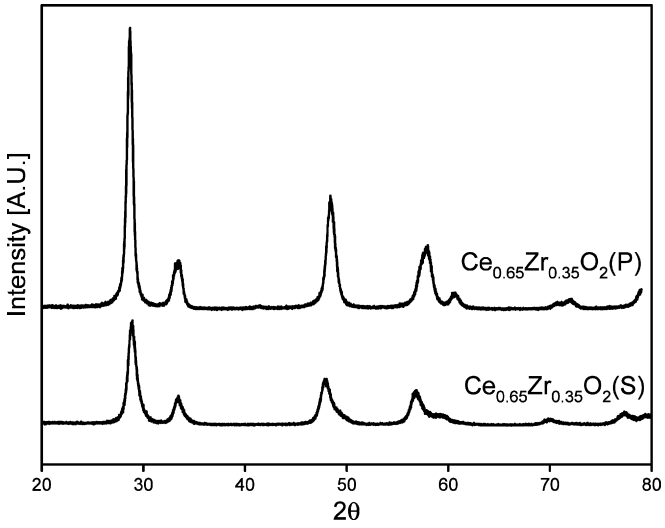

Fig. 7. XRD patterns of CeO_2–ZrO_2 mixed oxides calcined at 900 °C for 3 h.

the presence of defective structure in CeO_2–ZrO_2 mixed oxides [37,38]. Also, very weak bands at ca. 250–320 cm^{-1}, originating from the six Raman active modes ($A_{1g} + 2B_{1g} + 3E_g$) of tetragonal ZrO_2, could be observed in both cases [39]. The different intensity of the band in the two CeO_2–ZrO_2 mixed oxides may originate from the different degree of porosity ($Ce_{0.65}Zr_{0.35}O_2$(S): 0.285 cm^3/g, $Ce_{0.65}Zr_{0.35}O_2$(P): 0.070 cm^3/g).

From the results, Ce and Zr should be homogeneously distributed in CeO_2–ZrO_2 mixed oxides prepared by both supercritical synthesis and co-precipitation method. The distinct difference in the homogeneity of CeO_2–ZrO_2 mixed oxides between the two preparation methods was not observed.

3.4. The morphology change of Rh-loaded CeO_2–ZrO_2 on redox-aging

The SEM images and pore size distributions of CeO_2–ZrO_2 mixed oxides and Rh-loaded CeO_2–ZrO_2 mixed oxides before and after redox-aging were shown in Figs. 9 and 10, respectively. The pores seemed to be created from CeO_2–ZrO_2 mixed oxide nanoparticles when they were agglomerated, and the interstitial space between nanoparticles in the agglomeration might act as pores. In case of the supercritical synthesis, a lot of metal oxide nanoparti-

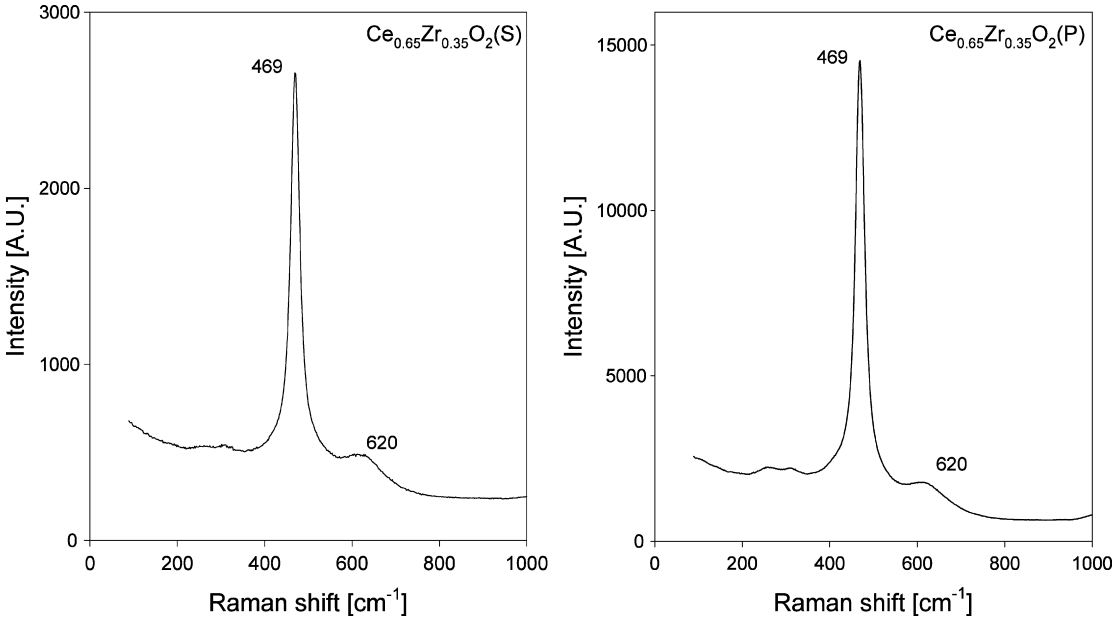

Fig. 8. Raman spectra of CeO_2–ZrO_2 mixed oxides.

cles might be precipitated very fast and the precipitated nanoparticles could be agglomerated rather coarsely due to the weak interaction between the oxide nanoparticles. The sparsely-agglomerated morphology and the large pores (>10 nm) could be expected in supercritical synthesis, as shown in Figs. 9a and 10a. In case of the co-precipitation method, precipitation and agglomeration of metal hydroxide nanoparticles could occur simultaneously and the precipitated nanoparticles could interact with each other. On dehydrating the metal hydroxide to metal oxide by calcination, the nanoparticles would interact more strongly with each other, and accordingly the densely-agglomerated morphology and the small pores (ca. 3 nm) could be obtained in co-precipitation method, as shown in Figs. 9b and 10b. It was shown that Rh impregnation on CeO_2–ZrO_2 mixed oxides did not affect their morphology (Figs. 9c, and 9d), while the smaller pore size was observed for Rh-loaded CeO_2–ZrO_2 mixed oxide prepared by supercritical synthesis (Fig. 10a). The pores with a diameter around 7 nm observed in the fresh Rh-loaded CeO_2–ZrO_2 prepared by the supercritical synthesis rather increased to near 30 nm after redox-aging, while the sparsely-agglomerated morphology was almost retained (Figs. 9e and 10a). On the other hand, the small pores around 3 nm and the densely-agglomerated morphology observed in the fresh Rh-loaded CeO_2–ZrO_2 prepared by the co-precipitation method were easily collapsed almost to complete sintering by redox-aging (Figs. 9f and 10b). The morphology change of Rh-loaded CeO_2–ZrO_2 mixed oxide was affected entirely by that of CeO_2–ZrO_2 mixed oxide.

3.5. The dispersion of Rh metal particles

The depth profiles of Rh in Rh-loaded CeO_2–ZrO_2 mixed oxides prepared by supercritical synthesis and co-precipitation method were measured by AES, as shown in Fig. 11. Agglomerated particles of CeO_2–ZrO_2 mixed oxides prepared by both synthesis methods were about several to tens micron-sized (observed from SEM image) and the incident electron beam of submicron-size in AES could be focused on an agglomerated particle. The powder samples were pressurized to a pellet form and the depth profile in an agglomerated particle could be obtained on sputtering the pellet by Ar ion beam in AES. It was observed from Fig. 11 that the composition of Rh in Rh-loaded CeO_2–ZrO_2 mixed oxides prepared by both synthesis methods remained almost constant over the submicron depth during sputtering. It indicated that Rh was dispersed relatively uniformly in the pores of CeO_2–ZrO_2 mixed oxides in both cases. But in case of co-precipitation method, Rh composition before sputtering was higher than that after sputtering and it implies that Rh was distributed in a higher fraction outside the pores rather than inside the pores due to the smaller pore size and its densely-agglomerated morphology, compared with supercritical synthesis.

Rh dispersion and Rh particle size of Rh-loaded CeO_2–ZrO_2 mixed oxides before and after redox-aging were shown in Table 4. The H_2 chemisorption at −80 °C and the O_2–CO_2–H_2–CO pulse method were used to determine the Rh dispersion. Because H_2 and CO interact with not only Rh but also CeO_2-related supports, the dispersions of Rh on CeO_2-related supports can be overestimated. Using the H_2 chemisorption at −80 °C proposed by Gatica et al. [26,27] and the O_2–CO_2–H_2–CO pulse method proposed by Takeguchi et al. [28], the interaction between adsorbates (H_2 or CO) and CeO_2-related support could be suppressed and more reliable measurements were obtained for Rh dispersion.

Rh dispersion measured by the H_2 chemisorption at −80 °C and the O_2–CO_2–H_2–CO pulse method was little different from each other but showed similar trend before and after redox-aging. Rh-loaded CeO_2–ZrO_2 mixed oxide prepared by co-precipitation method showed the very high Rh dispersion, compared with supercritical synthesis. This result was coincident with TPR results of Fig. 1 and Fig. 2, where the reduction peak around 500 °C for surface reduction of CeO_2–ZrO_2 mixed oxide prepared by co-precipitation method was completely shifted in spite of a low Rh loading of 0.05 wt%, in contrast with supercritical synthesis. Rh particle size was calculated from the assumption of hemispherical particles. Naturally, the larger Rh particle (ca. 3 nm) was calculated for Rh-loaded CeO_2–ZrO_2 mixed oxide prepared by supercritical synthesis, compared with co-precipitation method (ca. 1.5 nm). According to pore size distribution (Fig. 10a), the decrease of pore size was observed for Rh-loaded CeO_2–ZrO_2 mixed oxide prepared by supercritical synthesis and it might be due to the formation of the large Rh particle in the pore.

However, Rh-loaded CeO_2–ZrO_2 mixed oxide prepared by supercritical synthesis maintained relatively high Rh dispersion even after redox-aging. But in case of co-precipitation method, its Rh

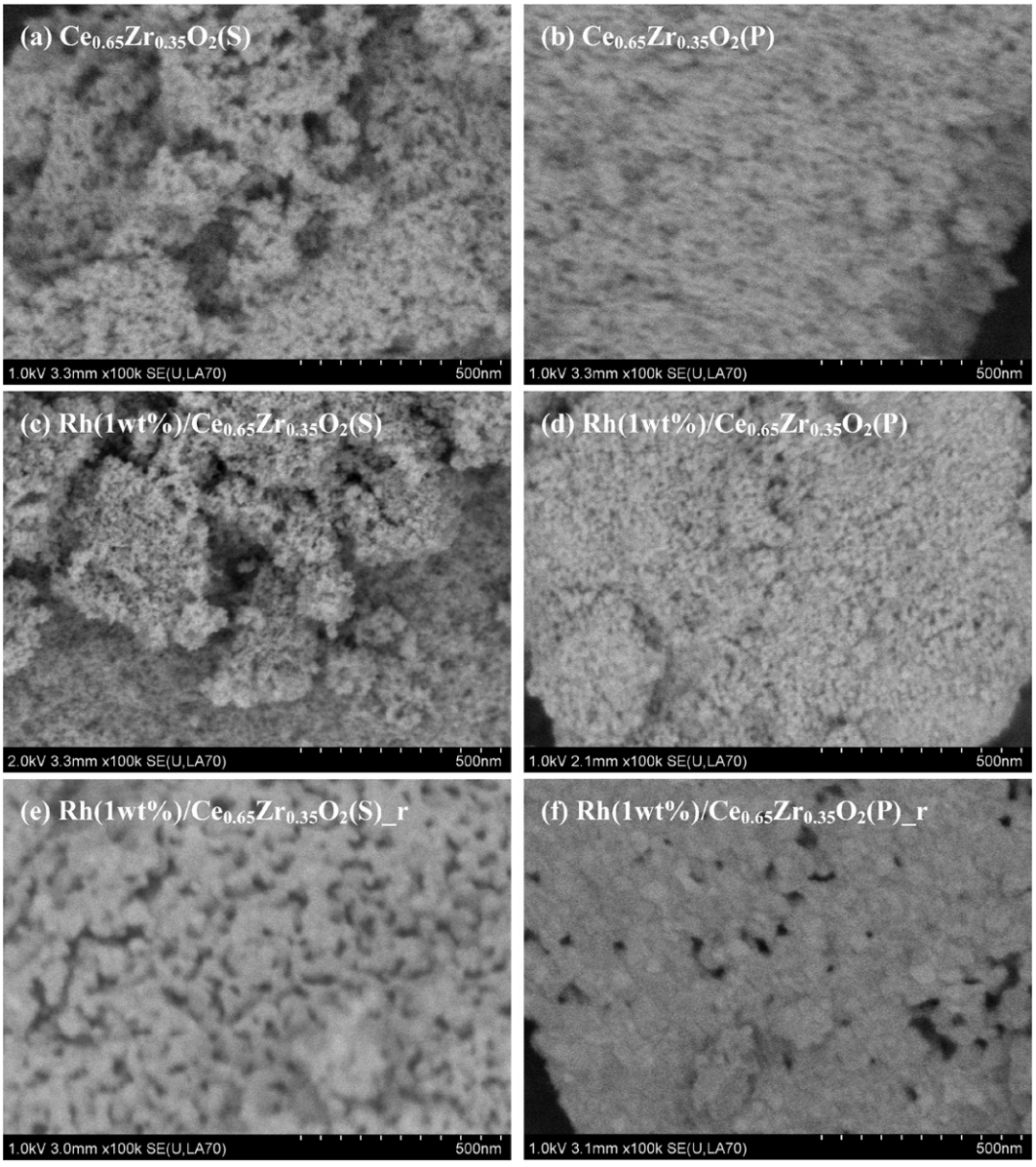

Fig. 9. SEM images of CeO_2–ZrO_2 mixed oxides and Rh-loaded CeO_2–ZrO_2 mixed oxides before and after redox-aging.

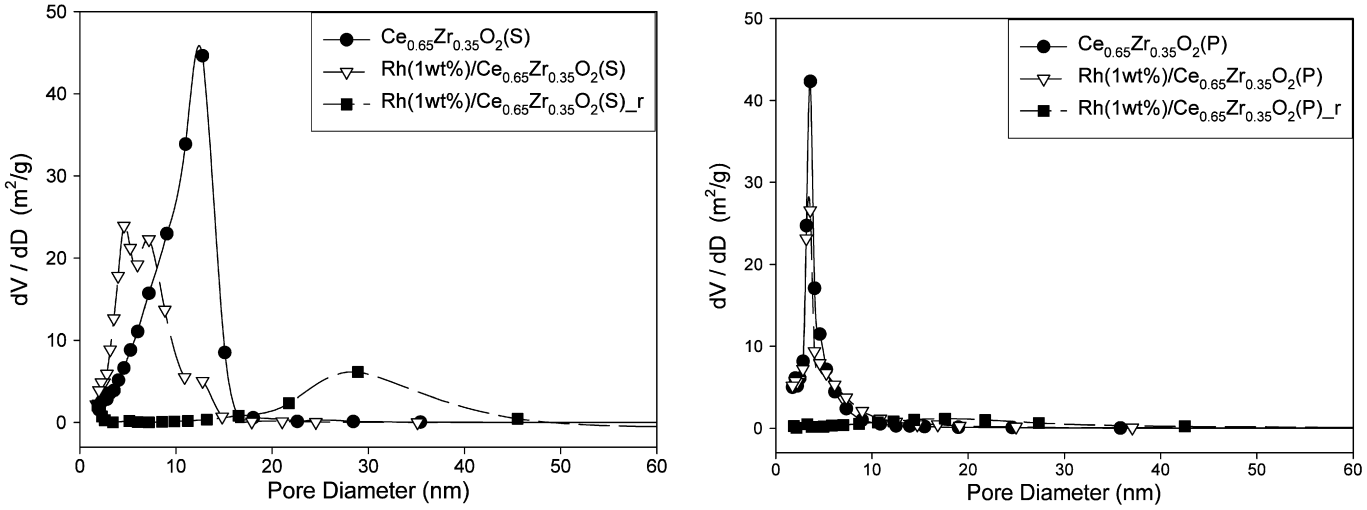

Fig. 10. Pore size distribution of CeO_2–ZrO_2 mixed oxides and Rh-loaded CeO_2–ZrO_2 mixed oxides before and after redox-aging.

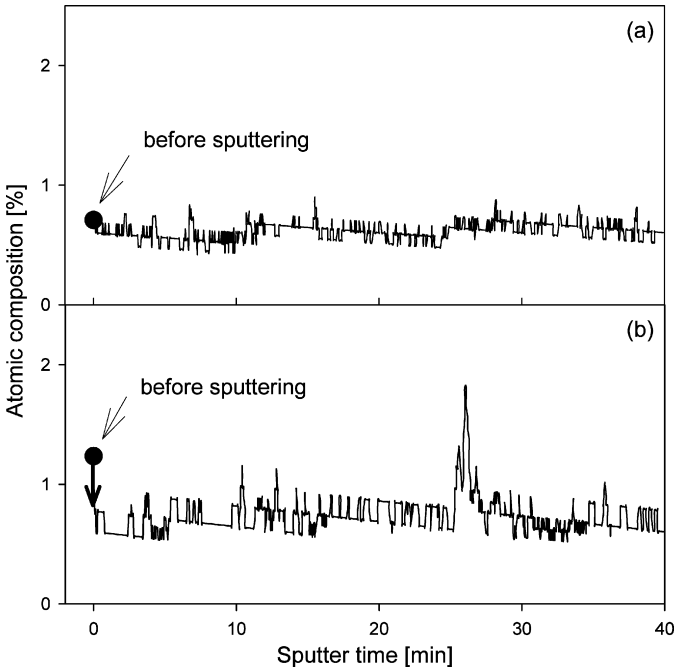

Fig. 11. Depth profiles of Rh in Rh-loaded CeO_2–ZrO_2 mixed oxides prepared by (a) supercritical synthesis and (b) co-precipitation method.

Table 4
Rh dispersion and Rh particle size of Rh-loaded CeO_2–ZrO_2 mixed oxides before and after redox-aging.

	Rh(1.00 wt%)/ $Ce_{0.65}Zr_{0.35}O_2$(S)		Rh(1.00 wt%)/ $Ce_{0.65}Zr_{0.35}O_2$(P)	
	Fresh	Aged	Fresh	Aged
Rh surface area (m^2/g_{cat})	1.69	0.66	3.93	0.22
Rh dispersion[a] (%)	38.3	14.9	89.4	4.9
Rh particle size[c] (nm)	2.9	7.3	1.2	22.0
Rh surface area (m^2/g_{cat})	1.50	0.60	2.73	0.20
Rh dispersion[b] (%)	34.1	13.5	62.0	4.6
Rh particle size[c] (nm)	3.2	8.1	1.8	24.2

[a] Measured by H_2 chemisorption at −80 °C.
[b] Measured by O_2–CO_2–H_2–CO pulse method.
[c] Calculated from the assumption of hemispherical particles (diameter).

dispersion decreased significantly after redox-aging in spite of very high Rh dispersion of the fresh sample. Rh-loaded CeO_2–ZrO_2 mixed oxide prepared by co-precipitation method encountered the collapse of pores during redox-aging and Rh particles in the pores must remain mostly in the bulk phase of CeO_2–ZrO_2 mixed oxide and not on the surface accessible to the atmosphere.

Rh-loaded CeO_2–ZrO_2 mixed oxide prepared by supercritical synthesis does not seem to be in a better position in view of Rh dispersion before redox-aging. But, for their practical application in three-way catalysts, Rh-loaded CeO_2–ZrO_2 mixed oxide is exposed to severe redox conditions at very high temperatures (>1000 °C) and its higher thermal stability for Rh dispersion could be more important factor as support of Rh catalyst.

It could be suggested that the densely-agglomerated morphology of Rh-loaded CeO_2–ZrO_2 mixed oxide prepared by co-precipitation method were easily collapsed almost to complete sintering by redox-aging and the pore collapse could prevent the lattice oxygen from migrating from the bulk to the atmosphere, leading to poor reducibility and thermal stability especially through redox-aging treatment, compared to those by supercritical synthesis. Also, the morphology could lead to great decrease of Rh dispersion after redox-aging. Accordingly, Rh-loaded CeO_2–ZrO_2 prepared by co-precipitation method showed poor activity and stability for the catalytic reduction of NO by CO.

It is noteworthy that high activity for the catalytic reduction of NO by CO as well as high surface area and Rh dispersion were retained after redox-aging in case of Rh-loaded CeO_2–ZrO_2 mixed oxide prepared by supercritical synthesis. CeO_2–ZrO_2 mixed oxide prepared by supercritical synthesis had more potential applications as catalyst support mainly due to its sparsely-agglomerated morphology and higher thermal stability.

4. Conclusions

CeO_2–ZrO_2 mixed oxides were prepared by supercritical synthesis and co-precipitation method, respectively, and they were used as support for Rh catalyst. The activities of Rh-loaded CeO_2–ZrO_2 catalysts were investigated for catalytic reduction of NO by CO and their physicochemical properties were characterized with TPR, N_2 adsorption, O_2-uptake, XRD, Raman, SEM, AES, and H_2/CO chemisorption. Discussions were made on the differences in the catalytic performances between the two preparation methods of CeO_2–ZrO_2 supports in terms of reducibility, homogeneity, morphology, Rh dispersion, and thermal stability. Rh-loaded CeO_2–ZrO_2 prepared by supercritical synthesis not only showed better reducibility, higher thermal stability, and superior performances for the catalytic reduction of NO by CO but also maintained relatively high Rh dispersion even after redox-aging, compared with co-precipitation method, due to its sparsely-agglomerated morphology. CeO_2–ZrO_2 mixed oxide prepared by supercritical synthesis had more potential applications as catalyst support mainly due to its sparsely-agglomerated morphology and higher thermal stability.

Acknowledgments

This research was supported by the Supercritical Fluid Technology Research Center from the Korea Energy Management Corporation and a grant from the Basic Research Program of the Korea Science and Engineering Foundation (Grant No. R01-2006-000-10765-0). The financial support from the Brain Korea 21 (BK21) program from the Korean Ministry of Education, Science and Technology Development was also kindly provided for this work.

References

[1] A. Trovarelli, C. de Leitenburg, M. Boaro, G. Dolcetti, Catal. Today 50 (1999) 353.
[2] H.S. Roh, K.W. Jun, S.E. Park, Appl. Catal. A Gen. 251 (2003) 275.
[3] B. Wen, M.Y. He, C. Costello, Energy Fuels 16 (2002) 1048.
[4] M. Flytzani-Stephanopoulos, T.L. Zhu, Y. Li, Catal. Today 62 (2000) 145.
[5] Y.W. Li, D.H. He, Q.M. Zhu, X. Zhang, B.Q. Xu, J. Catal. 221 (2004) 584.
[6] S. Imamura, Ind. Eng. Chem. Res. 38 (1999) 1743.
[7] S. Imamura, A. Doi, S. Ishida, Ind. Eng. Chem. Prod. Res. Dev. 24 (1985) 75.
[8] J. Kaspar, P. Fornasiero, M. Graziani, Catal. Today 50 (1999) 285.
[9] D. Terribile, A. Trovarelli, J. Llorca, J. Catal. 178 (1998) 229.
[10] J.R. Kim, W.J. Myeong, S.K. Ihm, Appl. Catal. B Environ. 71 (2006) 57.
[11] P. Fornasiero, R. Di Monte, R. Ranga, J. Kaspar, S. Meriani, A. Trovarelli, M. Graziani, J. Catal. 151 (1995) 168.
[12] G. Vlaic, P. Fornasiero, S. Geremia, J. Kaspar, M. Graziani, J. Catal. 168 (1997) 386.
[13] A. Trovarelli, C. de Leitenburg, G. Dolcetti, CHEMTECH 27 (1997) 32.
[14] H. Vidal, J. Kaspar, M. Pijolat, Appl. Catal. B Environ. 27 (2000) 49.
[15] T. Adschiri, K. Kanazawa, K. Arai, J. Am. Ceram. Soc. 75 (1992) 1019.
[16] T. Adschiri, K. Kanazawa, K. Arai, J. Am. Ceram. Soc. 75 (1992) 2615.
[17] P. Granger, F. Dhainaut, S. Pietrzik, P. Malfoy, A.S. Mamede, L. Leclercq, G. Leclercq, Top. Catal. 39 (2006) 65.
[18] T. Kolli, U. Lassi, K. Rahkamaa-Tolonen, T.J.J. Kinnunen, R.L. Keiski, Appl. Catal. A Gen. 298 (2006) 65.
[19] K. Thirunavukkarasu, K. Thirumoorthy, J. Libuda, C.S. Gopinath, J. Phys. Chem. B 109 (2005) 13272.
[20] T. Kolli, K. Rahkamaa-Tolonen, U. Lassi, A. Savimaki, R.L. Keiski, Catal. Today 100 (2005) 297.

[21] A.D. Sarkar, B. Khanra, J. Mol. Catal. A Chem. 229 (2005) 25.
[22] P. Granger, C. Dujardin, J.F. Paul, G. Leclercq, J. Mol. Catal. A Chem. 228 (2005) 241.
[23] A.B. Hungria, M. Fernandez-Garcia, J.A. Anderson, A. Martinez-Arias, J. Catal. 235 (2005) 262.
[24] H.O. Zhu, J.R. Kim, S.K. Ihm, Appl. Catal. B Environ. 86 (2009) 87.
[25] P. Fornasiero, J. Kaspar, M. Graziani, J. Catal. 167 (1997) 576.
[26] J.M. Gatica, R.T. Baker, P. Fornasiero, S. Bernal, G. Blanco, J. Kaspar, J. Phys. Chem. B 104 (2000) 4667.
[27] J.M. Gatica, R.T. Baker, P. Fornasiero, S. Bernal, J. Kaspar, J. Phys. Chem. B 105 (2001) 1191.
[28] T. Takeguchi, S. Manabe, R. Kikuchi, K. Eguchi, T. Kanazawa, S. Matsumoto, W. Ueda, Appl. Catal. A 293 (2005) 91.
[29] H.C. Yao, Y. Yu, J. Catal. 86 (1984) 254.
[30] M.F.L. Johnson, J. Mooi, J. Catal. 103 (1987) 502.
[31] G. Ranga Rao, P. Fornasiero, R. Di Monte, J. Kaspar, G. Vlaic, G. Balducci, S. Meriani, G. Gubitosa, A. Cremona, M. Graziani, J. Catal. 162 (1996) 1.
[32] P. Fornasiero, G. Ranga Rao, J. Kaspar, F. L'Erario, M. Graziani, J. Catal. 175 (1998) 269.
[33] R. Di Monte, P. Fornasiero, M. Graziani, J. Kaspar, J. Alloys Compd. 275–277 (1998) 877.
[34] S.T. Aruna, K.C. Patil, Nanostruct. Mater. 10 (1998) 955.
[35] A.S. Deshpande, M. Niederberger, Microporous Mesoporous Mater. 101 (2007) 413.
[36] D. Terribile, A. Trovarelli, J. Llorca, C. de Leitenburg, G. Dolcetti, Catal. Today 43 (1998) 79.
[37] R. Si, Y.W. Zhang, S.J. Li, B.X. Lin, C.H. Yan, J. Phys. Chem. B 108 (2004) 12481.
[38] M. Yashima, H. Arashi, M. Kakihana, M. Yoshimura, J. Am. Ceram. Soc. 77 (1994) 1067.
[39] E.F. Lopez, V.S. Escribano, M. Panizza, M.M. Carnasciali, G. Busca, J. Mater. Chem. 11 (2001) 1891.